Supplementary Materials for

Superconductivity in the doped Hubbard model and its interplay with next-nearest hopping t'

Hong-Chen Jiang* and Thomas P. Devereaux

*Corresponding author. Email: hcjiang@stanford.edu

Published 27 September 2019, *Science* **365**, 1424 (2019)
DOI: 10.1126/science.aal5304

This PDF file includes:

Supplementary Text

Numerical convergence

We have checked the numerical convergence of our DMRG simulations regarding spin rotational symmetry. It is known that in a finite-size system in one dimension or two dimensions, there can be no spontaneous breaking of continuous symmetry. Therefore, the *SU*(2) spin rotational symmetry of the Hubbard model Hamiltonian cannot be broken in the true ground state. This can be considered as one of the key signatures to determine whether a DMRG simulation has converged to the real ground state.

Our approach to address this issue takes two routes. First, we determine the expectation value of the z-component of the spin operator, i.e., $\langle S_i^z \rangle$, where *i* labels the lattice site. Since the ground state is an equal-weight superposition of $|S^z = 1/2\rangle$ and $|S^z = -1/2\rangle$ spin states, then $\langle S_i^z \rangle = 0$ for all sites *i*. A simple measurement of this condition is to define a quantity $m_z = \sum_{i=1}^{N} |\langle S_i^z \rangle| / N$, which should vanish as the DMRG simulation converges to the true ground state. In all of our DMRG simulations with t'=-0.25, we find that $m_z = 0$ even when we keep a relatively small number of states, as shown in Fig. S1, suggesting that our simulations have converged. Unfortunately, for t'=0, in which a much larger number (*m*=20000) of states are kept, a finite $m_z > 0$ is obtained, although it decreases rapidly with *m*. Second, the *SU*(2) spin rotational symmetry requires that the relation $\langle S_i^x S_j^x \rangle = \langle S_i^y S_j^y \rangle = \langle S_i^z S_j^z \rangle$ holds between two arbitrary sites *i* and *j*. This relation again is fulfilled in our simulations, which is contrary to the case of t'=0. In addition to spin rotational symmetry, other symmetries including both the lattice translational symmetry in $\hat{y}$ direction and reflection symmetry in $\hat{x}$ direction are also fulfilled. Therefore, we conclude that our simulation for t'=-0.25 has converged to the true ground state.

Further calculation details

To reliably describe ground state properties, we have explored the role of cylindrical size and boundary effects. In the current study we typically start our calculation with a random state. However, to elucidate the reliability of our results, we also check our calculations by adding a pinning field with the appropriate wavelength to stabilize a CDW state, for example. We find that in all the cases it is sufficient to add the pinning field during the initial sweeps of the calculation and ramp its amplitude to zero in a few subsequent sweeps. This happens only for the smallest number of states that we have considered, i.e., *m*=4096, while for the larger calculations with *m*>4096 it is not necessary to hold a finite (even vanishingly small) pinning field to stabilize the charge stripe pattern. This gives us the same results as we start from a completely random initial state without any pinning field, which undisputedly proves the reliability of our study. Moreover, there is no pinning pair-field to stabilize superconductivity throughout our DMRG calculation.

Ground state energy

In the insets of Fig. S2, we show examples of truncation error ϵ extrapolation of the energy per site $e_0 = E_0/N$, where E_0 is the total energy of a system with *N* lattice sites, for L_x=64 cylinders at doping level δ=12.5% and t'=-0.25 for *U*=8 (Fig. S2A) and *U*=12 (Fig. S2B). By keeping *m*=4096~20000 number of states, we are able to converge to the true ground state of the system by preserving all symmetries of the Hamiltonian,

including the *SU*(2) spin rotational symmetry, lattice translational symmetry in $\hat{y}$ direction and reflection symmetry in $\hat{x}$ direction. The truncation error extrapolation using a linear function with m=6000~20000 gives us e_0=-0.76583(1) for U=8 and e_0=-0.65104(1) for U=12. The ground state energy e_0 of other cylinders can be obtained similarly. Finally, we can obtain accurate estimates of the ground state energies in the long cylinder length limit, i.e., $L_x = \infty$, by carrying out finite-size scaling as a function of the inverse cylinder length. The extrapolation to the limit $L_x = \infty$ for doping level δ=12.5% is shown in Fig. S2, in which all energies for cylinder lengths L_x=16~64 for U=8 and L_x=16~64 for U=12 fall perfectly onto a linear fit, with a linear regression R^2 larger than 99.999%. This gives an energy e_0=-0.76965(2) for U=8, and e_0=-0.65409(1) for U=12 in the long cylinder limit $L_x = \infty$. For comparison, we have also obtained the ground state energy e_0=-0.7661(2) for U=8 and t'=0 in long cylinder limit, which is consistent with previous studies (3).

Convergence of superconducting correlations

Fig. S3A shows the SC pair-field correlation function $\Phi_{yy}(x)$ for x=1~32 in $\hat{x}$ direction on a L_x=64 cylinder by keeping m=4096~20000 states, at doping level δ=12.5%. The purple triangles label the extrapolated values to the limit ϵ=0, i.e., m=∞, using quartic polynomials, which is consistent with a power-law decay $\Phi_{yy}(x) \propto |x|^{-K_{sc}}$, as indicated by the red solid line.

Fig. S3B plots the extrapolated $\Phi_{yy}(L_x/2)$ on cylinders of length L_x=16~64 at doping level δ=12.5%, again fitted by different orders of polynomial functions. The black squares label the extrapolated $\Phi_{yy}(L_x/2)$ using a quartic polynomial (Poly4), while the red circles denote the results fitted by a quadratic polynomial, keeping up to m=10000 states (Poly2-small). For contrast, the blue triangles represent results fitted by the same quadratic polynomial function but only using 5 data points with the largest number of states (Poly2-large) for each cylinder. From the figure we can clearly see that both Poly4 and Poly2-large fittings are consistent with each other and enough to capture the long-distance behavior of the SC pair-field correlation, while the Poly2-small fitting by keeping up to m=10000 is not. This may explain the absence of long-range superconductivity in previous DMRG studies.

Finally, we have also calculated the 2-leg Hubbard ladder with U=8 and t'=0 at doping level δ=12.5%. The superconducting correlation $\Phi_{yy}(L_x/2)$ is shown in the inset of Fig. S3B. The extracted superconducting exponent K_{sc}=1.01(1) using system with length L_x=64~128, which is in excellent agreement with (14), providing additional evidence for the reliability of our study.

Friedel oscillations of the density profile and density-density correlation function

Alternatively, the exponent K_c can be extracted by fitting the Friedel oscillation, which is induced by the open boundaries of the cylinder, of the charge density distribution (25). In this work, we use $n(x) = n_0 + \delta n * \cos(2k_F x + \phi)x^{-K_c/2}$ to fit the local density profile to extract the Luttinger exponent K_c. Here, δn is the non-universal amplitude, ϕ is a phase shift, n_0 is the background density and k_F is the Fermi wavevector. An example is given in the inset of Fig. S4 for L_x=64 cylinder at doping level δ=12.5% with rung index x=1~L_x/2 by keeping m=20000 states. The main panel

shows the extracted value of K_c from the L_x=64 cylinder at the same doping level. In the limit of m=∞, the extracted exponent from L_x=64 cylinder is consistent with that determined from $A_{cdw}(L_x)$ as shown in Fig. 2.

Additional numerical check of the filled stripe phase

We have checked the t-t'-J model at doping level δ=12.5% and t=3J and t'=J/4 with a filled charge stripe ground state (20) and reached the same conclusion as for the Hubbard model at t'=0 with a true long-range CDW order (Fig. S5A) but with exponentially decaying SC pair-field correlation (Fig. S5B) (26).

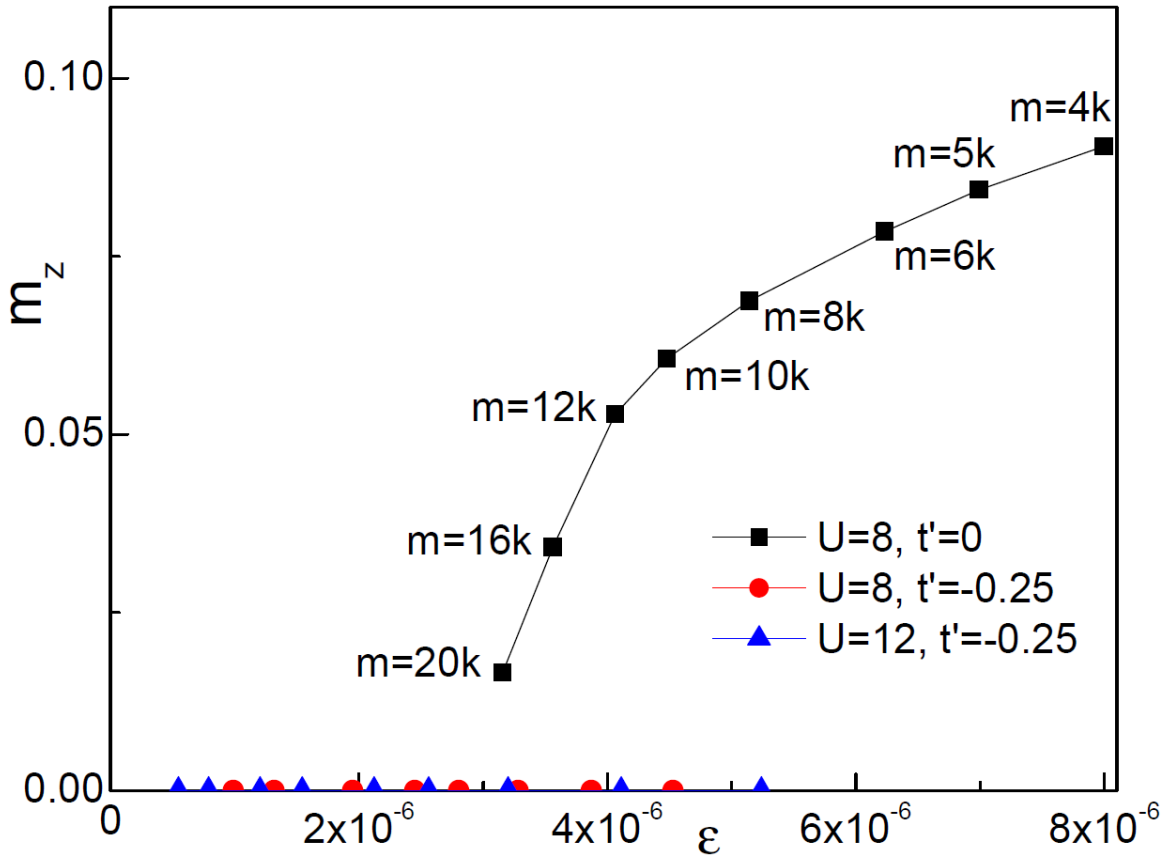

Fig. S1. Numerical convergence of Hubbard model. Magnetic moment $m_z = \frac{1}{N}\sum_{i=1}^{N}|\langle S_i^z\rangle|$ as a function of number of states m or truncation error ϵ of the Hubbard model at doping level δ=12.5% on L_x=64 cylinders for t'=0 and U=8 (black squares), t'=-0.25 and U=8 (red circles) and U=12 (blue triangles).

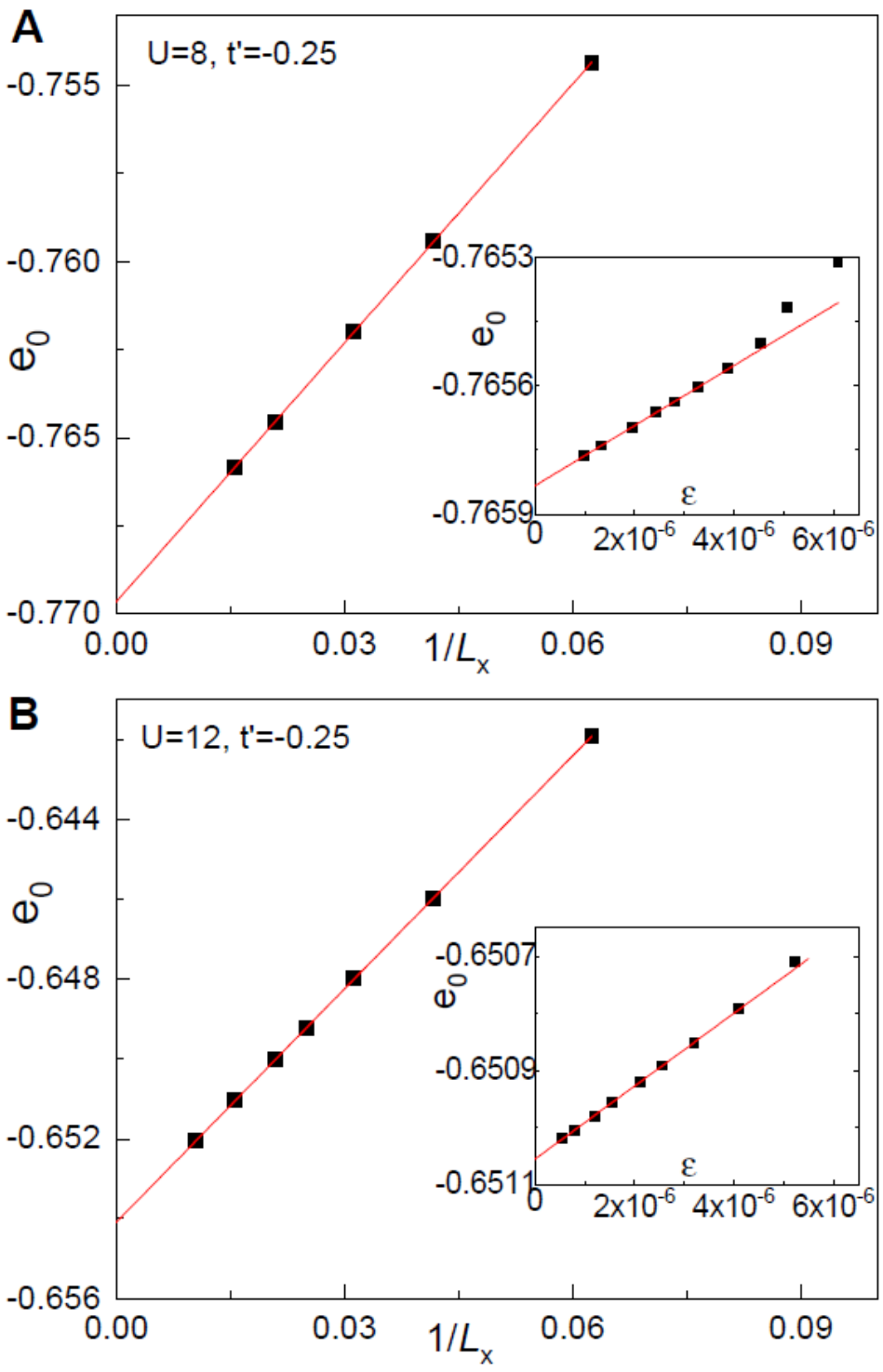

Fig. S2. Ground state energy of the Hubbard model. Ground state energy per site e_0 for δ=12.5% as a function of the inverse cylinder length L_x for (**A**) U=8 and (**B**) U=12. Insets: Examples of truncation error ϵ extrapolation of e_0 for L_x=64 cylinders at doping level δ=12.5% for (**A**) U=8 and (**B**) U=12. The red lines show the extrapolation using a linear function.

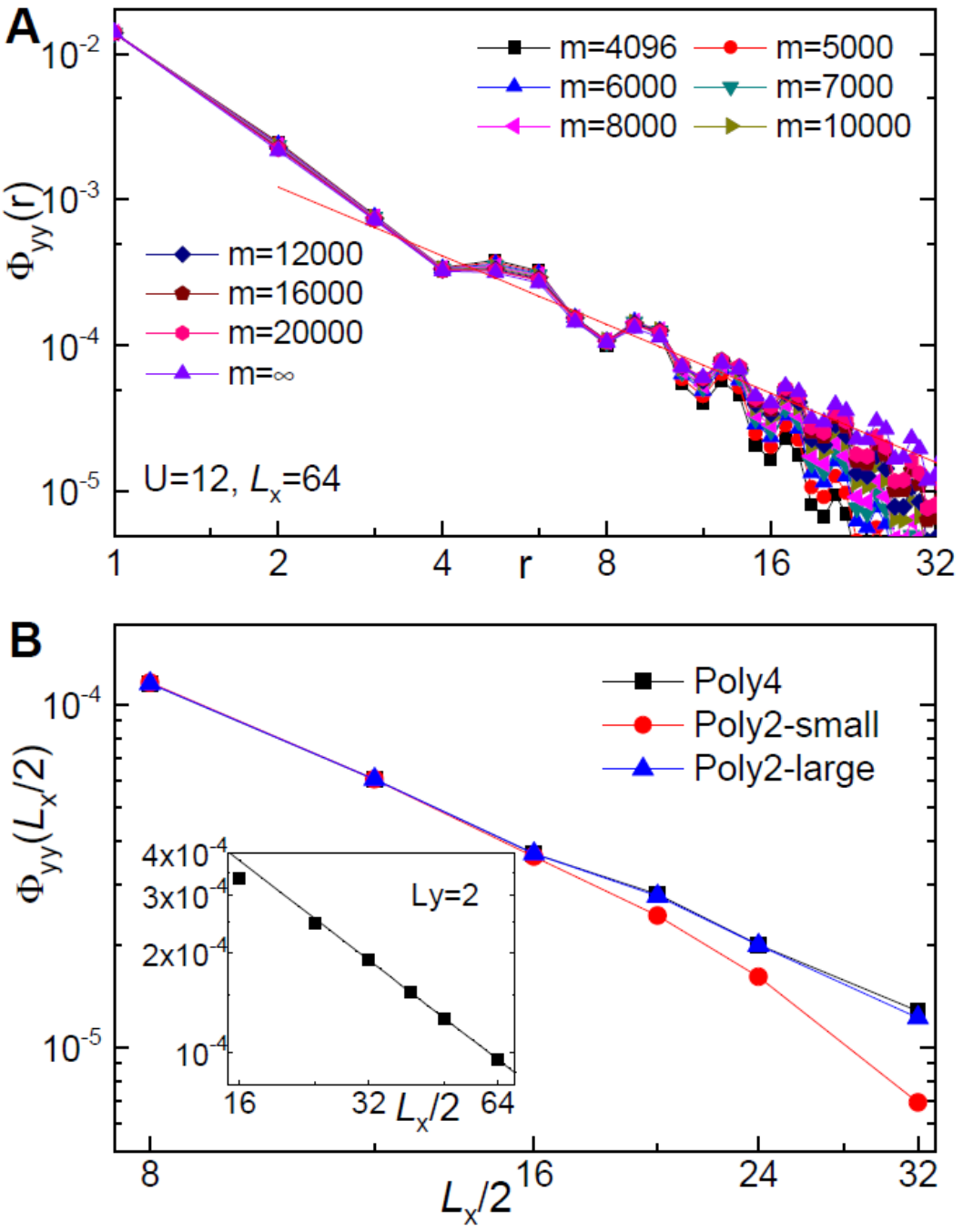

Fig. S3. Convergence of superconducting correlations. (**A**) SC correlation $\Phi_{yy}(r)$ on a L_x=64 cylinder for δ=12.5%, keeping m=4096~20000 states in the double-logarithmic plot, where r is the distance between two Cooper pairs in the $\hat{x}$ direction. The red line represents a power-law fit in the limit m=∞ with r=1~L_x/2. (**B**) Extrapolated $\Phi_{yy}(L_x/2)$ using a quartic polynomial (Poly4) and quadratic polynomial (Poly2) function in a double-logarithmic plot. Inset: The SC correlation $\Phi_{yy}(L_x/2)$ on a 2-leg Hubbard ladder for U=8 and t'=0 at doping level δ=12.5%.

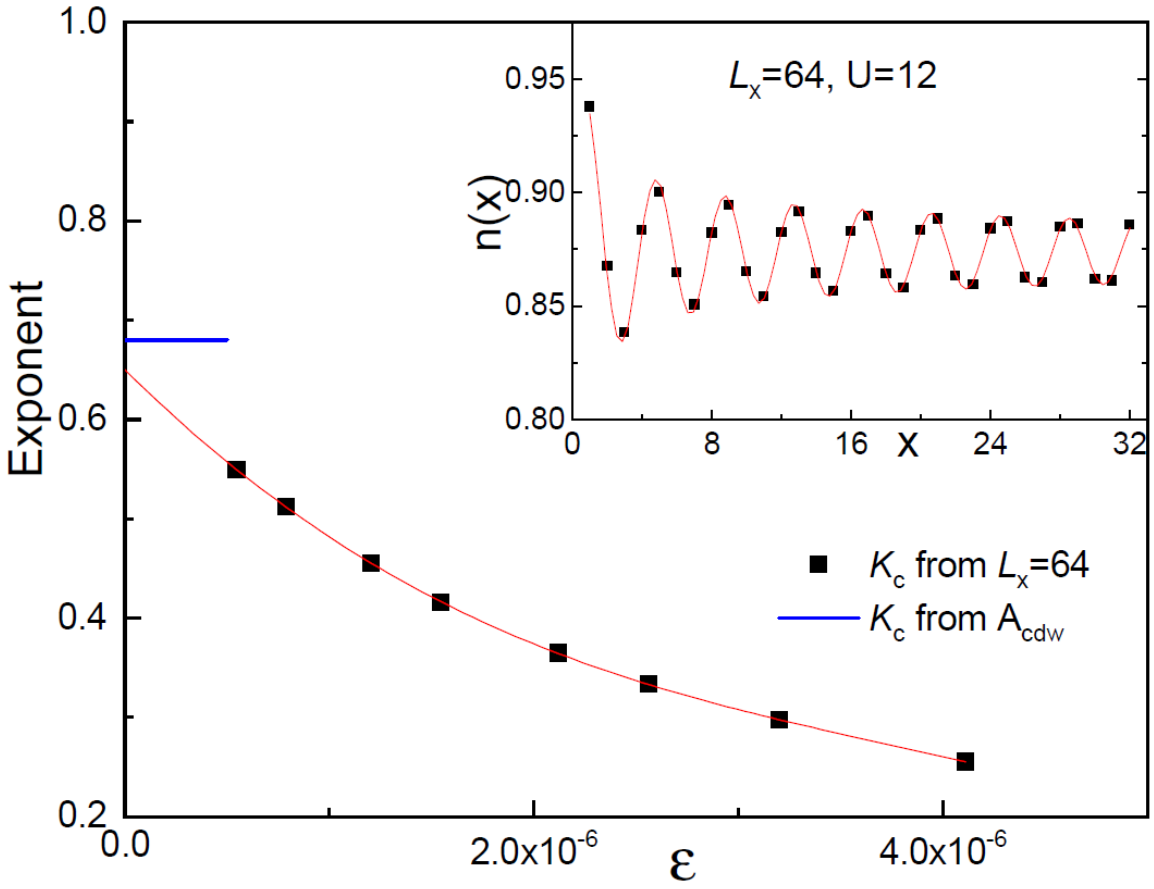

Fig. S4. Friedel oscillation of the charge density profile and Luttinger exponent K_c. Luttinger exponent K_c extracted from the local density profile $n(x)$ with Friedel oscillations on a L_x=64 cylinder for δ=12.5%, by keeping m=4096~20000 states. The blue line represents the exponents determined from $A_{cdw}(L_x)$. Inset: Fit of $n(x)$ (solid line) on a L_x=64 cylinder using function $n(x) = n_0 + \delta n * \cos(2k_F x + \phi)x^{-K_c/2}$ where x=1~$L_x/2$ is the rung index.

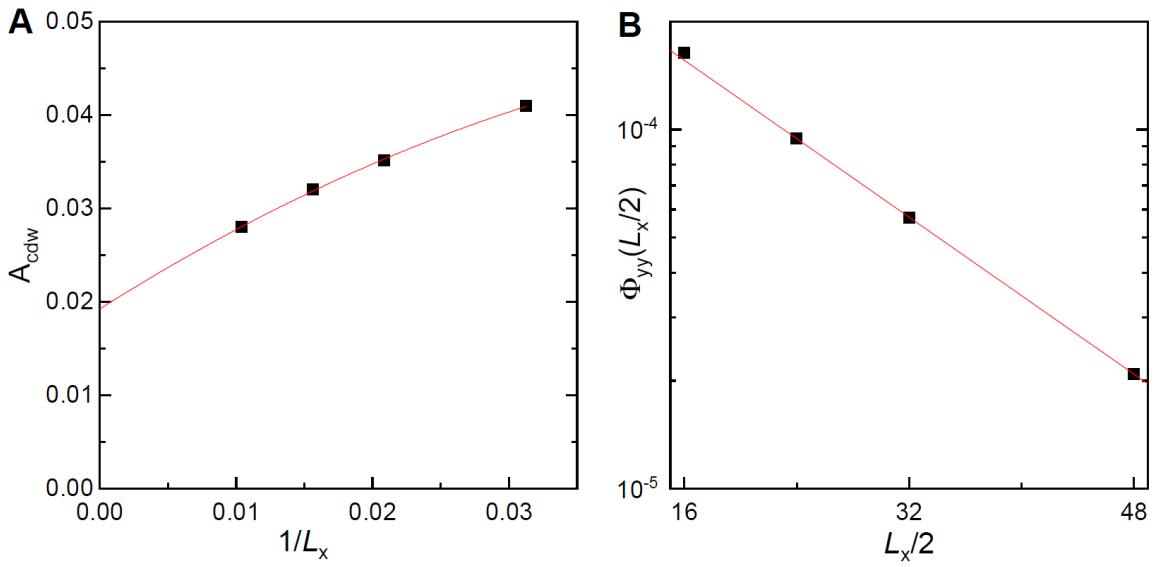

Fig. S5. The CDW and SC correlations in the filled stripe phase. Finite-size scaling of (**A**) the CDW amplitude $A_{cdw}(L_x)$ in double-linear scale and (**B**) the SC correlation function $\Phi_{yy}(L_x/2)$ in semi-logarithmic scale of the t-t'-J model at doping level δ=12.5% with $t = 3J$ and $t' = J/4$ with filled charge stripe ground state. The red line in (**A**) is the fit using second-order polynomial function and in (**B**) is the fit using exponential function.

References and Notes

1. P. Corboz, T. M. Rice, M. Troyer, Competing states in the *t-J* model: Uniform *D*-wave state versus stripe state. *Phys. Rev. Lett.* **113**, 046402 (2014). doi:10.1103/PhysRevLett.113.046402 Medline

2. P. Staar, M. Jiang, U. R. Hähner, T. C. Schulthess, T. A. Maier, Interlaced coarse-graining for the dynamic cluster approximation. *Phys. Rev. B* **93**, 165144 (2016). doi:10.1103/PhysRevB.93.165144

3. B.-X. Zheng, C.-M. Chung, P. Corboz, G. Ehlers, M.-P. Qin, R. M. Noack, H. Shi, S. R. White, S. Zhang, G. K.-L. Chan, Stripe order in the underdoped region of the two-dimensional Hubbard model. *Science* **358**, 1155–1160 (2017). doi:10.1126/science.aam7127 Medline

4. E. W. Huang, C. B. Mendl, S. Liu, S. Johnston, H.-C. Jiang, B. Moritz, T. P. Devereaux, Numerical evidence of fluctuating stripes in the normal state of high-T_c cuprate superconductors. *Science* **358**, 1161–1164 (2017). doi:10.1126/science.aak9546 Medline

5. G. Ehlers, S. R. White, R. M. Noack, Hybrid-space density matrix renormalization group study of the doped two-dimensional hubbard model. *Phys. Rev. B* **95**, 125125 (2017). doi:10.1103/PhysRevB.95.125125

6. E. W. Huang, C. B. Mendl, H. C. Jiang, B. Moritz, T. P. Devereaux, Stripe order from the perspective of the hubbard model. *npj Quantum Mater.* **3**, 22 (2018). doi:10.1038/s41535-018-0097-0

7. E. Pavarini, I. Dasgupta, T. Saha-Dasgupta, O. Jepsen, O. K. Andersen, Band-structure trend in hole-doped cuprates and correlation with $T_{c\,max}$. *Phys. Rev. Lett.* **87**, 047003 (2001). doi:10.1103/PhysRevLett.87.047003 Medline

8. A. Luther, V. J. Emery, Backward scattering in the one-dimensional electron gas. *Phys. Rev. Lett.* **33**, 589–592 (1974). doi:10.1103/PhysRevLett.33.589

9. E. Dagotto, J. Riera, D. Scalapino, Superconductivity in ladders and coupled planes. *Phys. Rev. B* **45**, 5744–5747 (1992). doi:10.1103/PhysRevB.45.5744 Medline

10. H. Tsunetsugu, M. Troyer, T. M. Rice, Pairing and excitation spectrum in doped *t-J* ladders. *Phys. Rev. B* **49**, 16078–16081 (1994). doi:10.1103/PhysRevB.49.16078 Medline

11. M. Troyer, H. Tsunetsugu, T. M. Rice, Properties of lightly doped *t-J* two-leg ladders. *Phys. Rev. B* **53**, 251–267 (1996). doi:10.1103/PhysRevB.53.251 Medline

12. E. Dagotto, T. M. Rice, Surprises on the way from one- to two-dimensional quantum magnets: The ladder materials. *Science* **271**, 618–623 (1996). doi:10.1126/science.271.5249.618

13. L. Balents, M. P. A. Fisher, Weak-coupling phase diagram of the two-chain Hubbard model. *Phys. Rev. B* **53**, 12133–12141 (1996). doi:10.1103/PhysRevB.53.12133 Medline

14. M. Dolfi, B. Bauer, S. Keller, M. Troyer, Pair correlations in doped hubbard ladders. *Phys. Rev. B* **92**, 195139 (2015). doi:10.1103/PhysRevB.92.195139

15. S. R. White, Density matrix formulation for quantum renormalization groups. *Phys. Rev. Lett.* **69**, 2863–2866 (1992). doi:10.1103/PhysRevLett.69.2863 Medline

16. See supplementary materials.

17. J. Zaanen, O. Gunnarsson, Charged magnetic domain lines and the magnetism of high-T_c oxides. *Phys. Rev. B* **40**, 7391–7394 (1989). doi:10.1103/PhysRevB.40.7391 Medline

18. K. Machida, Magnetism in La 2CuO 4 based compounds. *Physica C* **158**, 192–196 (1989). doi:10.1016/0921-4534(89)90316-X

19. H. J. Schulz, Incommensurate antiferromagnetism in the two-dimensional Hubbard model. *Phys. Rev. Lett.* **64**, 1445–1448 (1990). doi:10.1103/PhysRevLett.64.1445 Medline

20. H. C. Jiang, Z. Y. Weng, S. A. Kivelson, Superconductivity in the doped *t-J* model: Results for four-leg cylinders. *Phys. Rev. B* **98**, 140505 (2018). doi:10.1103/PhysRevB.98.140505

21. J. F. Dodaro, H.-C. Jiang, S. A. Kivelson, Intertwined order in a frustrated four-leg *t-J* cylinder. *Phys. Rev. B* **95**, 155116 (2017). doi:10.1103/PhysRevB.95.155116

22. P. Calabrese, J. Cardy, Entanglement entropy and quantum field theory. *J. Stat. Mech.* **2004**, P06002 (2004). doi:10.1088/1742-5468/2004/06/P06002

23. H.-C. Jiang, Data for "Superconductivity in the doped Hubbard model and its interplay with next-nearest hopping *t*'", version v2, Zenodo (2019); https://doi.org/10.5281/zenodo.3368664.

24. H.-C. Jiang, Source code for "Superconductivity in the doped Hubbard model and its interplay with next-nearest hopping *t*'", version 1, Zenodo (2019); https://doi.org/10.5281/zenodo.2651698.

25. S. R. White, I. Affleck, D. J. Scalapino, Friedel oscillations and charge density waves in chains and ladders. *Phys. Rev. B* **65**, 165122 (2002). doi:10.1103/PhysRevB.65.165122

26. Prior results on two-leg ladders indicate filled charge stripes with one hole per each charge-stripe unit cell, with simultaneous long-range decay of SC correlations, yielding a LE liquid (*14*). This is distinguished from the results obtained on four-leg Hubbard and *t-J* ladders, where filled stripes do not support long-range SC correlations (*3*).